Yu. A. Bykov, Candidate of Technical Sciences

A. Podgorny Institute of Mechanical Engineering Problems of NASU, Kharkiv, Ukraine,
e-mail: bykow@ipmach.kharkov.ua

Ключові слова: *чисельне моделювання течії, аеропружність в турбомашинах, нестаціонарна течія, нестаціонарні навантаження.*

UDC 621.625+621.438

HIGHER ORDER NUMERICAL METHOD FOR AEROELASTIC PROBLEMS

Запропоновано метод чисельного моделювання течії в'язкого стисливого газу через решітку коливних лопаток. Метод призначений для інтегрування нестаціонарних двовимірних рівнянь Нав'є-Стокса, усереднених за Рейнольсом, які доповнюються рівнянням моделювання турбулентності. Метод має локально третій порядок апроксимації по просторових координатах та часу. З використанням методу проведено чисельний аналіз аеропружних характеристик решітки турбінних профілів 4-ї стандартної конфігурації в трансзвуковому потоці. Здійснено зіставлення отриманих результатів з даними чисельного моделювання з використанням методів другого і першого порядку апроксимації, а також з даними експерименту.

Introduction

The solution of the aeroelasticity problem involves solving the unsteady aerodynamic problem, which consumes a significant amount of computing resources. The accuracy and detail of the solution to the problem affect the accuracy of determining the conditions for the possible onset of uncontrolled oscillations.

A lot of papers are devoted to improving the methods for solving the aerodynamic problem. The most popular method of simplification is the solution to the stationary problem of modeling flow followed by a solution to one-dimensional piston motion problem for determining unsteady loads on a blade surface [1]. Further, according to the degree of simplification, there follows the method of harmonic balance [2], which involves solving the aerodynamic problem in a frequency domain followed by a solution of the system of linear equations for determining the conditions for the possible onset of oscillations. In some cases, the solution of the Euler equations of fluid motion [3] or the time-linearized Navier-Stokes equations [4] are considered admissible simplifications. Comparing the results of different approaches to solving the aerodynamic problem [5], one can see that the most accurate and detailed data are obtained by solving the unsteady Navier-Stokes equations. Such an approach is rather widely used for solving the problems of aeroelasticity in turbomachines [6], including the use of implicit schemes [7]. The accuracy of the solution obtained depends mainly on the order of approximation of the basic equations. An increased accuracy of the simulation is necessary for complex flows in which shocks waves are present, i.e. in trans- and supersonic flows. This work presents the results of transonic flow simulation in the cascade of oscillating turbine profiles using methods of different accuracy, and a quantitative evaluation of the correspondence of the results depending on the order of approximation.

Numerical method

The numerical method is based on the approved explicit modified numerical scheme of Godunov-Kolgan [6], which has a second order of approximation for spatial variables. The scheme integrates two-dimensional, Reynolds-averaged Navier-Stokes equations:

$$\frac{\partial \mathbf{U}}{\partial t}+\frac{\partial \mathbf{F}}{\partial x}+\frac{\partial \mathbf{G}}{\partial y}=\mathbf{0} \tag{1}$$

$$\mathbf{U}=\begin{bmatrix}\rho\\ \rho v_1\\ \rho v_2\\ e\end{bmatrix},\quad \mathbf{F}=\begin{bmatrix}\rho v_2\\ \rho v_1 v_2-\tau_{21}\\ p+\rho v_2^2-\tau_{22}\\ (p+e)v_2-v_1\tau_{21}-v_2\tau_{22}-\lambda\dfrac{\partial T}{\partial x_2}\end{bmatrix},\ \mathbf{G}=\begin{bmatrix}\rho v_1\\ p+\rho v_1^2-\tau_{11}\\ \rho v_1 v_2-\tau_{12}\\ (p+e)v_1-v_1\tau_{11}-v_2\tau_{12}-\lambda\dfrac{\partial T}{\partial x_1}\end{bmatrix}.$$

Here **U** is the vector of conservative variables, **F** and **G** are the fluxes of conservative variables in *x* and *y* coordinates, respectively. Equations (1) are complemented by equations of the Wilcox turbulence model *k*-ω [8]:

$$\frac{\partial}{\partial t}(\rho k)+\frac{\partial}{\partial x_i}(\rho k v_i-(\mu+\sigma_k\mu_T)\frac{\partial k}{\partial x_i})=\Pi-\beta^*\rho\omega k$$

$$\frac{\partial}{\partial t}(\rho\omega)+\frac{\partial}{\partial x_i}(\rho\omega v_i-(\mu+\sigma_\omega\mu_T)\frac{\partial \omega}{\partial x_i})=\alpha\frac{\omega}{k}\Pi-\beta\rho\omega^2 \qquad (2)$$

$$\mu_T=\rho\frac{k}{\omega},\ \Pi=\tau_{ij}^T S_{ij}.$$

Equations (1) and (2) are integrated according to the modified explicit Godunov scheme [6], which is well approved in the calculation of various types of compressible fluid flows [9]. The scheme is designed for the use of arbitrary non-structural grids. In this paper, we used a moving O-grid of quadrilateral cells.

For integrating the initial equations, the following schemes for approximating the unknown variables were used:

- the original Godunov scheme of a first-order approximation, in which the variables take constant values within one cell: $u_{i\pm0.5}=u_i$ (here $u_{i\pm0.5}$ – values on the cell faces, u_i – values in the cell centers);
- схема the Godunov-Kolgan scheme having a locally second-order approximation of the equations, the variables being represented as a linear function within the cell: $u_{i\pm0.5}=u_i\pm\frac{h}{2}(u_\xi)_i$, $(u_\xi)_i\approx\min\text{ mod}\left\{\frac{\Delta_i u}{h},\frac{\Delta_{i+1}u}{h}\right\}$, $\Delta_i u=u_i-u_{i-1}$ (here $(u_\xi)_i$ – approximation of the first derivative of the variable);
- the ENO decomposition, proposed in [10], which has a second order approximation of the equations and uses the second derivative of the variable:

$$(u_\xi)_i\approx\min\text{ mod}\left\{\frac{\Delta_i u}{h_i}+\alpha h_i\min\text{ mod}[\Delta\Delta_{i-1}u,\Delta\Delta_i u],\frac{\Delta_{i+1}u}{h_{i+1}}-\beta h_{i+1}\min\text{ mod}[\Delta\Delta_i u,\Delta\Delta_{i+1}u]\right\},$$

$$u_{i\pm0.5}=u_i\pm\frac{h}{2}(u_\xi)_i,\ \Delta\Delta_i u=\frac{1}{h^2}(\Delta_{i+1}u-\Delta_i u),\ \alpha=\beta=0.5;$$

- the ENO decomposition, which has a locally third order approximation of the equations (here the indices *i* and *j* denote the corresponding values in the centre of the cell, the indices *i*±0.5 and *j*±0.5 denote the values on the cell faces):

$$u\approx u_{i,j}+\Delta x(u_x)_{i,j}+\Delta y(u_y)_{i,j}+\frac{1}{2}\Delta x^2(u_{xx})_{i,j}+\frac{1}{2}\Delta y^2(u_{yy})_{i,j}+\Delta x\Delta y(u_{xy})_{i,j}$$

$$(u_x)_{i-0.5,j-0.5}=f(u_{i,j},u_{i-0.5,j},u_{i,j-0.5},x_{i,j},x_{i-0.5,j},x_{i,j-0.5},y_{i,j},y_{i-0.5,j},y_{i,j-0.5})$$

$$(u_{xx})_{i-0.5,j-0.5}=f((u_x)_{i,j},(u_x)_{i-0.5,j},(u_x)_{i,j-0.5},x_{i,j},x_{i-0.5,j},x_{i,j-0.5},y_{i,j},y_{i-0.5,j},y_{i,j-0.5})$$

$$(u_x)_{i,j}=\min\text{ mod}[(u_x)_{i-0.5,j-0.5},(u_x)_{i+0.5,j+0.5}]$$

$$(u_{xx})_{i,j}=\min\text{ mod}[(u_{xx})_{i-0.5,j-0.5},(u_{xx})_{i+0.5,j+0.5}]$$

$$\Delta x=x-x_{i,j},\ \Delta y=y-y_{i,j}.$$

To achieve a third-order approximation in integrating a quadratic representation of variables on the cell faces is used, for which the values of the variables are determined at two points having coordinates:

$$\xi_{P1} = \frac{1}{2} - \frac{1}{\sqrt{12}}, \xi_{P2} = \frac{1}{2} + \frac{1}{\sqrt{12}},$$

where ξ takes the values in the range [0,1] within one cell face.

Integration of equations (1, 2) in the time domain is carried out using the third order Runge-Kutta scheme:

$$u^{(1)} = u^n + \Delta t L\left(u^n\right)$$
$$u^{(2)} = \frac{3}{4}u^n + \frac{1}{4}u^{(1)} + \frac{1}{4}\Delta t L\left(u^{(1)}\right).$$
$$u^{n+1} = \frac{1}{3}u^n + \frac{2}{3}u^{(2)} + \frac{2}{3}\Delta t L\left(u^{(2)}\right)$$

Object of study

A cascade of turbine profiles was chosen as a study object, which was examined at the École Polytechnique Fédérale de Lausanne [11]. The cascade is better known as '4th standard configuration'. The cascade was flowed by air with the following parameters: total pressure p_0 = 205.8 kPa, outlet pressure p_2 = 98.4 kPa, flow stagnation temperature T_0 = 300 K, incidence angle β = –45°. The chosen mode is characterized by the Mach number M_2 = 1.2 and presence of a complex shock wave pattern both on the blade suction side and in the inter-blade passage. The blades performed bending vibrations with an amplitude 0.0038 of the chord and a frequency of 150 Hz. The phase difference between the blades was 0 and 180 degrees. Fig. 1 shows the appearance of the cascade, Fig. 2 shows the Schlieren picture of the flow in the cascade for the M_2 = 1.2 mode, on which the position and intensity of the shock waves is clearly visible.

The flow simulation was performed during the 1.5 period of the profile oscillations. The initial conditions were the results of a steady flow simulation in the cascade. The calculation was carried out for two values of the phase shift of the oscillations between the blades: σ = 0° and σ = 180°.

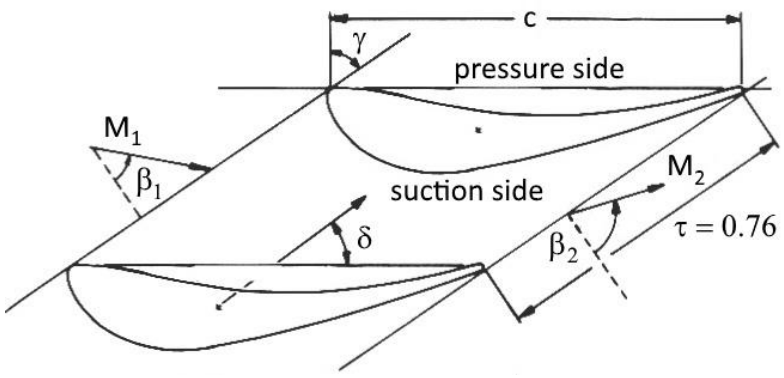

Fig. 1. Turbine blade cascade of the 4th standard configuration:
c – chord length; M_1 – inlet velocity; M_2 – outlet velocity; β_1 – inlet flow angle; β_2 – outlet flow angle; γ – chordal stagger angle; δ – bending vibration direction; τ – dimensionless blade pitch

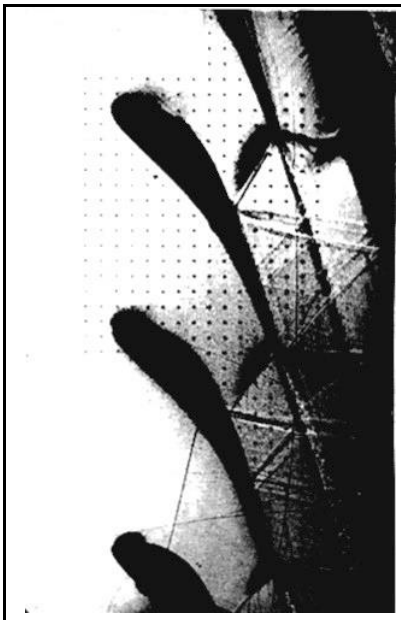

Fig. 2. Schlieren picture of the flow in the turbine blade cascade

Results and discussion

Fig. 3 shows the distribution of the average pressure over the profile surface (hereinafter, the values of x/c in the range of 0−1 correspond to the profile suction side, the values in the range of 1 − 2 – to the pressure side). The graph clearly shows the presence of a shock wave on the suction side in region $x/c = 0.7$. Hereinafter, the results for different approximation schemes are marked by the following symbols: 'Godunov' – for the Godunov scheme of a first order, 'G-K' – for the Godunov-Kolgan scheme of a locally second order, 'ENO 2' for a second order ENO scheme, 'ENO 3' – for a third order ENO scheme, squares – the results of the experiment from [11].

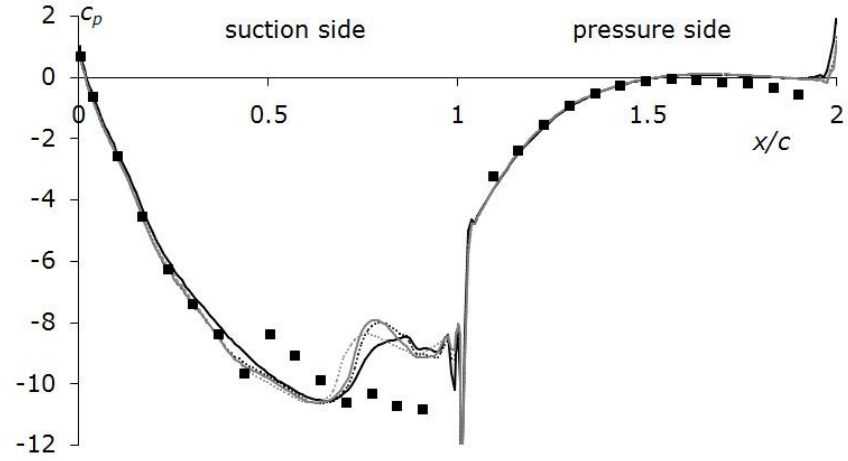

Fig. 3. Distribution of the time-averaged pressure along the profile surface
—— – 'Godunov'; ····· – 'G-K'; —— – 'ENO 2'; ····· – 'ENO 3'; ■ – experiment

When analyzing Fig. 3 in detail, one can see that a first and second order schemes predict the position of a shock wave at the same point with the difference in intensity, while a third-order scheme shifts the position of the wave upstream. All the schemes do not show the presence of a reflected wave from the trailing edge of the adjacent profile, which is to be at position $x/c = 0.5$. Fig. 4 shows the contour lines of the pressure in the inter-blade passage, which can clarify the shock wave distribution pattern.

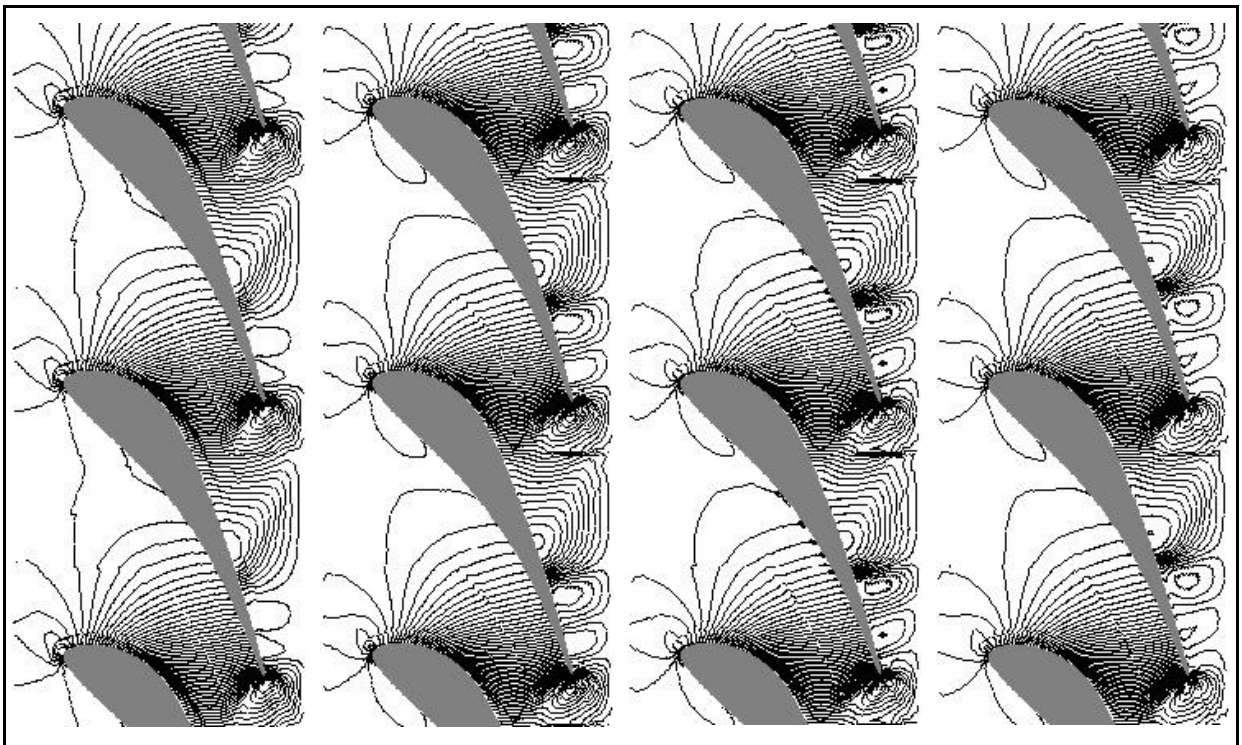

Fig. 4. Contour lines of the pressure in the inter-blade passage:
a — 'Godunov'; b — 'G-K'; c — 'ENO 2'; d — 'ENO 3'

Instead of the shock wave distribution pattern shown in Fig. 2, only two shock waves are observed — on the pressure side in the trailing edge region, and on the suction side — in region $x/c = 0.7$, which are scattered toward the middle of the inter-blade passage. The pictures in Fig. 4 show an increase in the intensity of shock waves as the scheme order increases, the position of the waves with increasing order shifts upstream too. Further, unsteady results for the inter-blade phase shift σ = 0° are presented in the form of a first harmonic amplitude of the unsteady pressure distribution along the profile $p_n(x) = \frac{\sqrt{C_1^{a\,2}(x) + C_1^{b\,2}(x)}}{(p_0 - p_1)h_0 c}$ (Fig. 5). Here $C_1^a(x), C_1^b(x)$ is the distribution of the first coefficients of the Fourier expansion for the unsteady pressure.

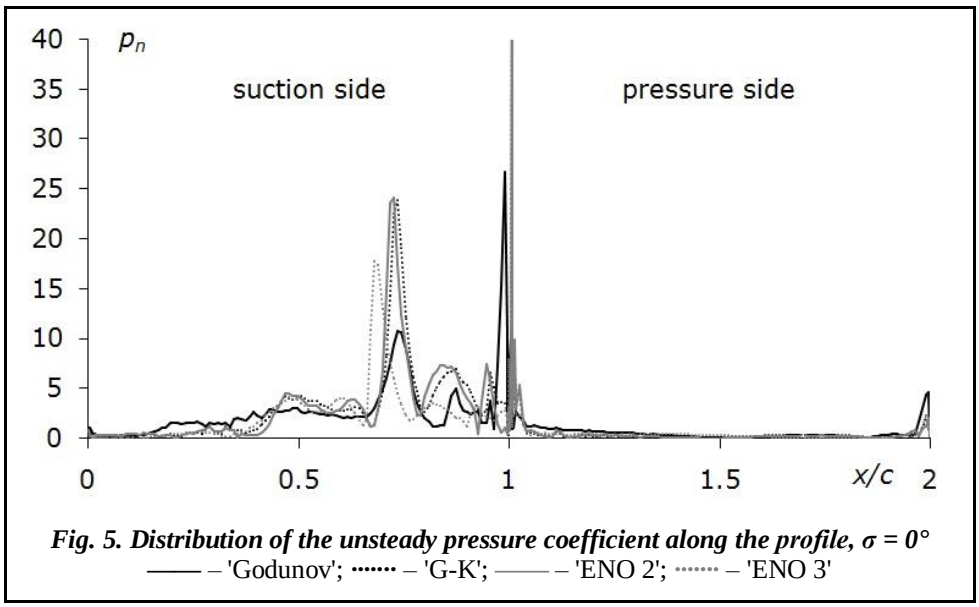

Fig. 5. Distribution of the unsteady pressure coefficient along the profile, σ = 0°
—— – 'Godunov'; ····· – 'G-K'; —— – 'ENO 2'; ····· – 'ENO 3'

A thorough analysis of the results presented shows that the maxima of values in region $x/c = 0.7$ correspond to the position of the shock wave for each variant. Fig. 6 also shows the distribution of the phase shift between the unsteady pressure first harmonic and the profile oscillation $phi(x) = \text{arctg}\frac{C_1^b(x)}{C_1^a(x)}$.

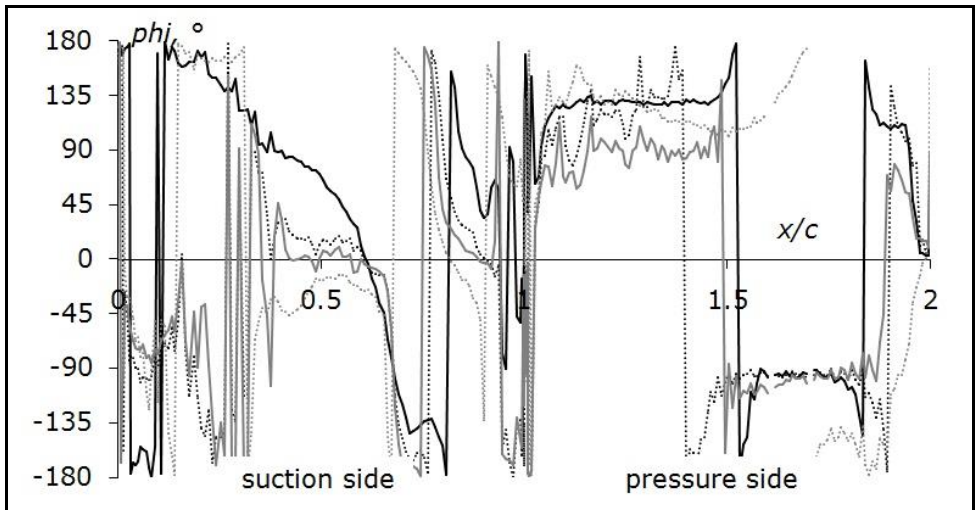

Fig. 6. Distribution of the unsteady pressure phase shift along the profile, σ = 0°
—— – 'Godunov'; ····· – 'G-K'; —— – 'ENO 2'; ····· – 'ENO 3'

The form of the pressure oscillation phase distribution along the profile is preserved for all the calculation variants. A more significant indicator for aeroelastic characteristics is the work distribution of the aerodynamic forces $A(x)=\frac{C_1^a(x)\boldsymbol{wn}}{(p_0-p_1)\pi c^2 h_0^2}$ (here $\boldsymbol{w}$ is the velocity of a point movement along the profile, $\boldsymbol{n}$ is the normal to the profile surface) along the profile surface, which is shown in Fig. 7.

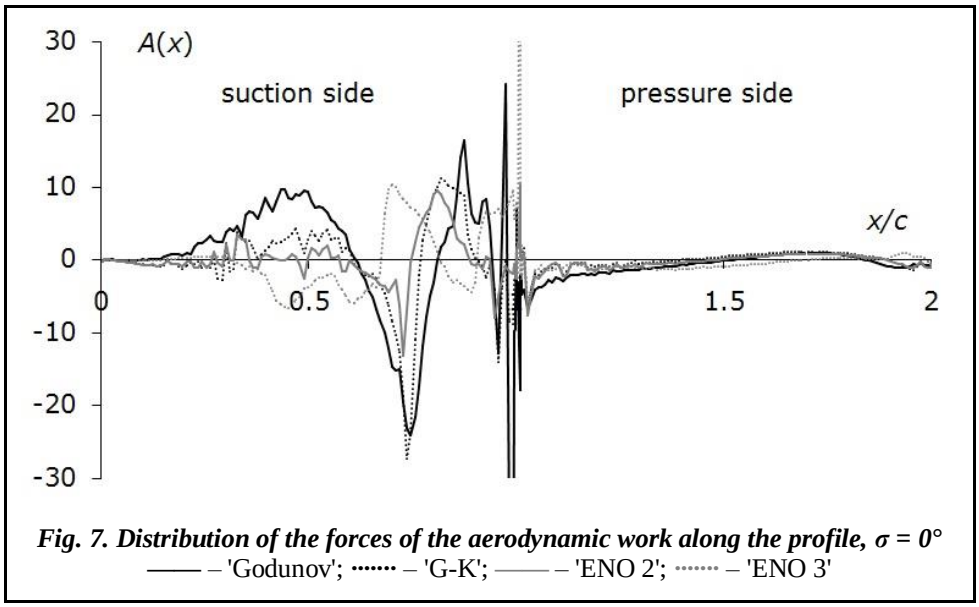

Fig. 7. Distribution of the forces of the aerodynamic work along the profile, σ = 0°
—— – 'Godunov'; ····· – 'G-K'; —— – 'ENO 2'; ····· – 'ENO 3'

The graph in Fig. 7 allows us to see that the maxima of values in region $x/c = 0.7$ correspond to the shock wave position for each calculation variant, however, in region $x/c = 0.5$, work for the first and the third order scheme differs in sign, while for the second order scheme it is close to zero.

Further, in Fig. 8 the unsteady results for the inter-blade phase shift σ = 180° are shown in the form of the first harmonic amplitude distribution of the unsteady pressure along the profile. For this mode of operation, there exist experimental data, which are represented in the graphs by squares.

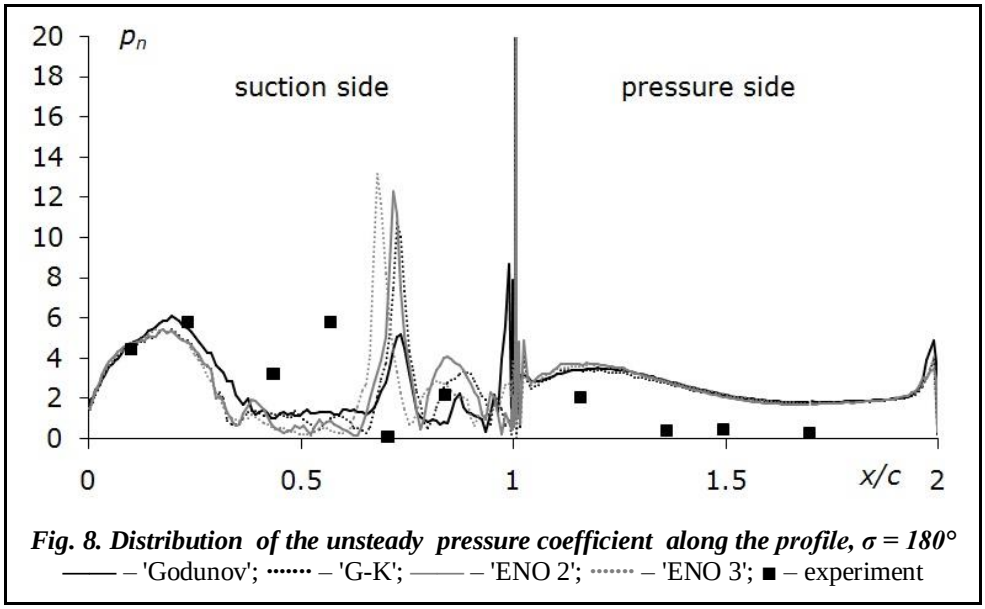

Fig. 8. Distribution of the unsteady pressure coefficient along the profile, σ = 180°
—— – 'Godunov'; ····· – 'G-K'; —— – 'ENO 2'; ····· – 'ENO 3'; ■ – experiment

An analysis of the results presented shows that the maxima of the values in region $x/c = 0.7$ correspond to the shock wave position for each variant of calculation. At the same time, the values of calculations in region $x/c = 0.5$ do not correspond to the experiment in which a reflected shock wave was detected in this

region. The values in region $x/c = 0 - 0.3$ agree well enough with the experimental data. Fig. 9 also shows the distribution of phase shift between the unsteady pressure of the first harmonic and the profile oscillation.

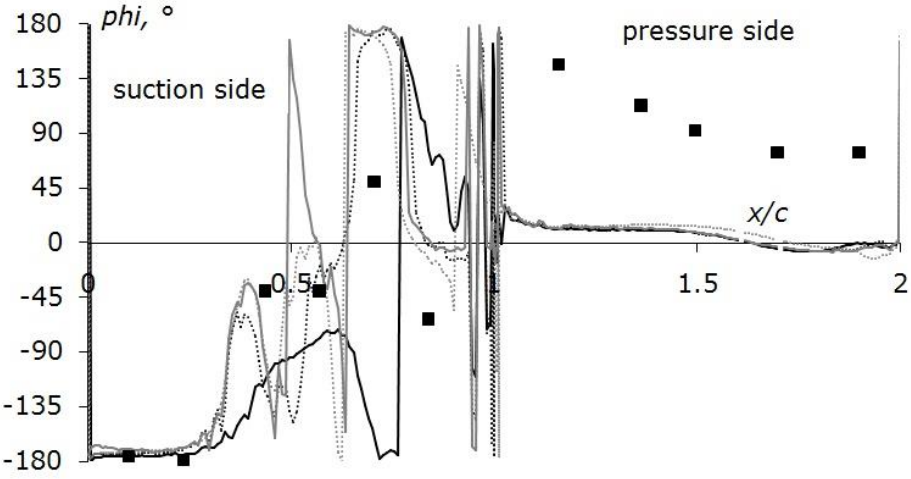

Fig. 9. Distribution of unsteady pressure phase shift along profile, σ = 180°°
—— – 'Godunov'; ····· – 'G-K'; —— – 'ENO 2'; ····· – 'ENO 3'; ■ – experiment

On the suction side, the calculated data are in good agreement with the experimental ones, even in region $x/c = 0.5$, which has no shock wave in the calculation. The phase value in region $x/c = 0.5$ takes negative values, which corresponds to the positive work of the aerodynamic forces, whereas in the region of shock wave $x/c = 0.7$ it passes through 180° and takes positive values, working on damping oscillations. Thus, there are two regions whose influences compensate each other. Fig. 10 shows the distribution of the work of the aerodynamic forces for the variant of calculation σ = 180°.

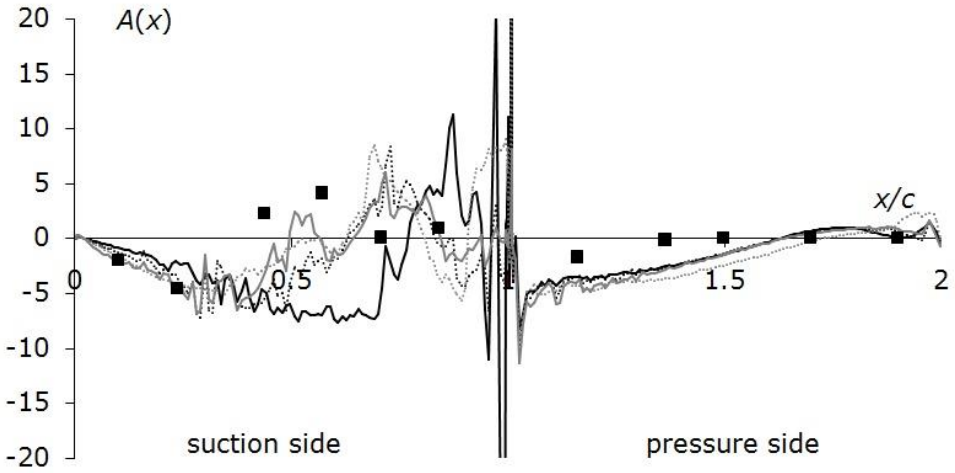

Fig. 10. Distribution of the work of the aerodynamic forces along the profile, σ = 180°
—— – 'Godunov'; ····· – 'G-K'; —— – 'ENO 2'; ····· – 'ENO 3'; ■ – experiment

In Fig. 10 one can observe a satisfactory agreement of the data in the range of $x/c = 0-0.3$, and the difference in the maxima positions related to the position of the shock wave. Also, one can observe a significant difference in the data of the first-order scheme, which take predominantly negative values.

The accuracy of the above-mentioned results is considerably dependent on the order of numerical scheme approximation. When unsteady processes are simulated, this difference can affect the character of the aeroelastic behavior of the blade cascade, predicting excitation instead of the possible damping and vice versa. Also of great importance in applying higher order methods is the use of grids adapted to the characteristic

features of the flow. The absence of grid thickening both in the region of the first shock wave and in the inter-blade passage has led to the wave dissipation and significant distortion of the numerical results, regardless of the scheme order.

Conclusions

An algorithm for numerical simulation of gas flow through a cascade of oscillating profiles with an increased approximation order is presented. The algorithm is designed to solve the aeroelasticity problems in the turbomachine cascades. A numerical analysis of transonic flow through the cascade of turbine profiles is carried out. It is shown that the numerical simulation of complex transonic flows requires the application of methods with increased accuracy. These methods make it possible to improve the resolution of any scheme. Unsteady characteristics of complex transonic flows also depend significantly on the approximation order of variables. An insufficient order of approximation can sometimes lead to a significant distortion of the results, right up to the sign change in the work of the aerodynamic forces. Along with the application of higher order schemes, it is necessary to use adaptive computational grids, which take into account the flow features and do not introduce additional errors to the region of large gradients of values.

References

1. Brouwer K., Crowell A. R., McNamara J. J. Rapid Prediction of Unsteady Aeroelastic Loads in Shock-Dominated Flows. Proc. of 56th AIAA/ASCE/AHS/ASC Structures, Structural Dynamics, and Materials Conf. 2015. – P. 1–20.
2. Padmanabhan M. A., Pasiliao C. L., Dowell E. H. Simulation of Aeroelastic Limit-Cycle Oscillations of Aircraft Wings with Stores. *AIAA J*. 2014. Vol. 52. No 10. P. 2291–2299.
3. Chen T., Xu M., Xie L. Aeroelastic Modeling Using Geometrically Nonlinear Solid-Shell Elements. *AIAA J*. 2014.Vol 52. No 9. P 1980–1993.
4. Kersken H. , Frey C., Voigt C., Ashcroft G. Time-Linearized and Time-Accurate 3D RANS Methods for Aeroelastic Analysis in Turbomachinery. *ASME. J. Turbomach*. 2012. Vol. 134(5). P. 051024-051024-8.
5. Gupta K. K., Voelker L. S. Aeroelastic Simulation of Hypersonic Flight Vehicles. *AIAA J*. 2012. Vol. 50, No 3. P. 717–723.
6. Gnesin V. I., Bykov Yu. A. Numerical Investigation of Aeroelastic Characteristics of Turbine Rotor in Off-Design Mode *J. of Mech. Eng*. 2004. Vol. 1. No 7, P 31–40.
7. Gendel S., Gottlieb O., Degani D. Fluid–Structure Interaction of Elastically Mounted Slender Body at High Incidence *AIAA J*. 2015. Vol. 53. No 5. P. 1309–1318.
8. Wilcox D. C. Reassessment of the Scale-Determining Equation for Advanced Turbulence Models. *AIAA J*. 1988. Vol. 26. No 11. P. 1299–1310.
9. Yershov S. V., Bykov Yu. A., Smulsky Ya. I., Sharov K. A., Terekhov V. I. Numerical and Experimental Investigation of Backward-Facing Step Flow with Passive Flow Con, K. A trol. *Visnyk NTU "KhPI".* 2013. No 56. P. 199–203.
10. Rusanov A. V., Yershov S. V. Mathematical Modeling of Unsteady Gas-Dynamic Processes in the Flowing Parts of Turbomachines.Kharkov: IPMash NASU, 2008. – 275 p.
11. Bolcs A., Fransson T. H. Aeroelasticity in Turbomachines. Comparison of Theoretical and Experimental Cascade Results. Communication du Laboratorie de Thermique Appliquee et de Turbomachines, Lausanne, EPFL. 1986. №13. – 230 p.

Received 20 November 2017